

SLIM: A Well-Conditioned Single-Source Boundary Element Method for Modeling Lossy Conductors in Layered Media

Shashwat Sharma, *Student Member, IEEE*, and Piero Triverio, *Senior Member, IEEE*

Abstract—The boundary element method (BEM) enables the efficient electromagnetic modeling of lossy conductors with a surface-based discretization. Existing BEM techniques for conductor modeling require either expensive dual basis functions or the use of both single- and double-layer potential operators to obtain a well-conditioned system matrix. The computational cost is particularly significant when conductors are embedded in stratified media, and the expensive multilayer Green's function (MGF) must be used. In this work, a novel single-source BEM formulation is proposed, which leads to a well-conditioned system matrix without the need for dual basis functions. The proposed single-layer impedance matrix (SLIM) formulation does not require the double-layer potential to model the background medium, which reduces the cost associated with the MGF. The accuracy and efficiency of the proposed method are demonstrated through realistic examples drawn from different applications.

Index Terms—Electromagnetic modeling, boundary element method, surface integral equations, single-source formulations.

I. INTRODUCTION

THE need for full-wave electromagnetic (EM) modeling of lossy conductors arises in many applications. The design of high-speed on-chip interconnects requires an accurate prediction of signal propagation and cross-talk, which is heavily influenced by the frequency-dependent variation of skin depth [1]. Likewise, the quantification of losses in the sub-wavelength unit cells of metasurfaces and metamaterials requires modeling conductors as imperfect [2].

Electromagnetic modeling of lossy conductors with the finite element method [3] or volume integral equations [4]–[6] requires an extremely fine volumetric discretization of the structure to capture skin effect at high frequencies. In contrast, the boundary element method (BEM), which is based on a surface integral representation of Maxwell's equations [7], requires meshing only on the interfaces between objects. This reduction of dimensionality allows capturing the skin effect without the need for an extremely fine mesh, making the BEM an appealing approach for modeling penetrable media.

Conductor modeling with the BEM requires describing an interior problem to capture the physics within objects,

and an exterior problem to model coupling between them. Approximate techniques for the interior problem such as the Leontovich surface impedance boundary condition (SIBC) [8] are not accurate near corners or at low frequencies, where skin effect has not yet developed. The generalized impedance boundary condition (GIBC) [9] and related formulations [10], [11] are well conditioned and applicable over a broad frequency range, but require both single- and double-layer potential operators [12] for modeling the exterior problem. When conductors are embedded in stratified background media, the multilayer Green's function (MGF) [13] is required for computing the single-layer potential, and its curl is required for the double-layer potential [13]. Both the MGF and its curl are several times more expensive to compute than the homogeneous Green's function. Therefore, having to compute both the single- and double-layer operators for layered media has a significant cost, and increases code complexity. Other methods such as the enhanced augmented electric field integral equation (eAEFIE) [14] require not only the same operators as the GIBC, but also the use of expensive dual basis functions [15] to obtain a well-conditioned system matrix [16].

The differential surface admittance (DSA) approach [17]–[20] is a single-source formulation which requires only the single-layer potential operator of the exterior problem. However, the DSA formulation also leads to an ill-conditioned system matrix unless dual basis functions are employed [21], [22]. A single-source impedance-based (SSI) formulation was proposed as a remedy [23], but the resulting system matrix is still not as well conditioned as the GIBC.

In this work, a novel single-source formulation is proposed, which offers the advantages of both the GIBC and the DSA, while overcoming their shortcomings. Like the DSA, the proposed single-layer impedance matrix (SLIM) formulation involves only a differential electric current density as the source [17]. Therefore, the SLIM approach does not require the double-layer potential operator for the exterior problem, unlike the GIBC, which leads to a smaller matrix fill time. Furthermore, the SLIM formulation leads to a well-conditioned system matrix without the need for dual basis functions, unlike the DSA or SSI approaches.

II. PROPOSED FORMULATION

In the following, time-harmonic fields with a time dependence of $e^{j\omega t}$ are assumed, where ω is the cyclical frequency and $j = \sqrt{-1}$. Primed coordinates represent source points,

Accepted to the IEEE Antennas and Wireless Propagation Letters (Volume: 19, Issue: 12, Dec. 2020, DOI: 10.1109/LAWP.2020.3022593).

S. Sharma and P. Triverio are with the Edward S. Rogers Sr. Department of Electrical & Computer Engineering, University of Toronto, Toronto, ON, M5S 3G4 Canada, e-mails: shash.sharma@mail.utoronto.ca, piero.triverio@utoronto.ca.

This work was supported by the Natural Sciences and Engineering Research Council of Canada (Collaborative Research and Development Grants program), by Advanced Micro Devices, and by CMC Microsystems.

while unprimed coordinates represent observation points. We first consider a structure composed of a single object occupying volume \mathcal{V} , bounded by a surface \mathcal{S} with outward unit normal vector \hat{n} . The proposed method will be generalized to structures with multiple objects in Section II-C. The object is assumed to be homogeneous with permittivity ε , permeability μ , and electrical conductivity σ . The object may be embedded in a layered medium, where the l^{th} layer is denoted by \mathcal{V}_l , has permittivity ε_l and permeability μ_l . We define $\mathcal{V}_0 = \bigcup_{l=1}^{N_l} \mathcal{V}_l$. The system may be excited with an incident plane wave, $[\vec{E}_{\text{inc}}(\vec{r}), \vec{H}_{\text{inc}}(\vec{r})]$, $\vec{r} \in \mathcal{V}_0$, or through lumped ports [24], resulting in a field distribution $[\vec{E}(\vec{r}), \vec{H}(\vec{r})]$ for $\vec{r} \in \mathcal{V}$.

A. Interior Problem

1) *Original Configuration*: The tangential electric and magnetic fields on \mathcal{S} can be related via the magnetic field integral equation (MFIE) [7],

$$j\omega\varepsilon\hat{n} \times \mathcal{L} \left[\hat{n}' \times \vec{E}(\vec{r}') \right] (\vec{r}) + \hat{n} \times \mathcal{K} \left[\hat{n}' \times \vec{H}(\vec{r}') \right] (\vec{r}) - \frac{1}{2} \hat{n} \times \vec{H}(\vec{r}) = 0 \quad (1)$$

for $\vec{r}, \vec{r}' \in \mathcal{S}$. Using the MFIE (1) rather than the electric field integral equation (EFIE) will lead to better conditioning of the final system matrix. Definitions of the integro-differential operators \mathcal{L} and \mathcal{K} may be found in literature [7], and involve the homogeneous Green's function of the object's material.

A triangular mesh is generated for the surface of the object. Equation (1) is discretized by expanding $\hat{n} \times \vec{E}(\vec{r})$ and $\hat{n} \times \vec{H}(\vec{r})$ with RWG basis functions [25] and tested with rotated $\hat{n} \times$ RWG functions. This leads to the matrix equation

$$-j\omega\varepsilon \mathbf{L} \mathbf{E} - \left(\mathbf{K} - \frac{1}{2} \mathbf{I}_\times \right) \mathbf{H} = \mathbf{0}, \quad (2)$$

where \mathbf{L} and \mathbf{K} are the discretized \mathcal{L} and \mathcal{K} operators. For highly conductive media, specialized integration routines must be used for assembling \mathbf{L} and \mathbf{K} , to capture the fast oscillations of the Green's function [9], [14]. Matrix \mathbf{I}_\times is the identity operator obtained by testing RWG with $\hat{n} \times$ RWG functions. Column vectors \mathbf{E} and \mathbf{H} contain the coefficients of the basis functions associated with $\hat{n} \times \vec{E}(\vec{r})$ and $\hat{n} \times \vec{H}(\vec{r})$, respectively.

2) *Equivalent Configuration*: Next, we use the surface equivalence principle [26] to replace the conductive object with the background material in which it resides, while requiring that $\hat{n} \times \vec{E}(\vec{r})$ remains unchanged for $\vec{r} \in \mathcal{S}$ [17]. An equivalent electric current density, \vec{J}_Δ ,

$$\vec{J}_\Delta(\vec{r}) = \hat{n} \times \vec{H}(\vec{r}) - \hat{n} \times \vec{H}_{\text{eq}}(\vec{r}), \quad (3)$$

must be introduced on \mathcal{S} to keep fields in \mathcal{V}_0 unchanged. In (3), $\hat{n} \times \vec{H}_{\text{eq}}(\vec{r})$ is the tangential magnetic field on \mathcal{S} in the equivalent configuration. Enforcing an unchanged tangential electric field will later avoid the need for the double-layer potential operator of the exterior problem [17].

Vector fields \vec{J}_Δ , $\hat{n} \times \vec{H}(\vec{r})$ and $\hat{n} \times \vec{H}_{\text{eq}}(\vec{r})$ are now expanded with RWG basis functions to obtain the discrete version of (3),

$$\mathbf{J}_\Delta = \mathbf{H} - \mathbf{H}_{\text{eq}}, \quad (4)$$

where column vectors \mathbf{J}_Δ and \mathbf{H}_{eq} contain the coefficients of the basis functions associated with \vec{J}_Δ and $\hat{n} \times \vec{H}_{\text{eq}}(\vec{r})$, respectively.

In the equivalent configuration, the $\hat{n} \times \vec{E}(\vec{r})$ and $\hat{n} \times \vec{H}_{\text{eq}}(\vec{r})$ can also be related via the EFIE [7], which after discretization reads

$$j\omega\mu_l \mathbf{L}_l \mathbf{H}_{\text{eq}} - \left(\mathbf{K}_l - \frac{1}{2} \mathbf{I}_\times \right) \mathbf{E} = \mathbf{0}, \quad (5)$$

where \mathbf{L}_l and \mathbf{K}_l are the discretized \mathcal{L} and \mathcal{K} operators involving the homogeneous Green's function associated to \mathcal{V}_l .

B. Exterior Problem

To enable broadband simulations of multiscale objects, the augmented EFIE (AEFIE) [27] is employed to model the exterior problem. The charge density ρ_Δ associated to \vec{J}_Δ is introduced as an additional unknown, and discretized with pulse basis functions [27]. The total electric field tangential to \mathcal{S} is written in discretized form as

$$jk_0 \mathbf{L}_m^{(A)} \mathbf{J}_\Delta + c_0 \mathbf{D}^T \mathbf{L}_m^{(\phi)} \mathbf{B} \rho_\Delta + \eta_0^{-1} \mathbf{I}_\times \mathbf{E} = \eta_0^{-1} \mathbf{E}_{\text{inc}}, \quad (6)$$

where $\mathbf{L}_m^{(A)}$ and $\mathbf{L}_m^{(\phi)}$ are the discretized vector and scalar potential parts of the \mathcal{L} operator, respectively, and ρ_Δ contains coefficients of ρ_Δ . Subscript m indicates that the multilayer Green's function of the stratified background medium is used. Column vector \mathbf{E}_{inc} is related to the incident electric field. Quantities k_0 , η_0 , and c_0 are, respectively, the wave number, wave impedance, and speed of light in free space. The differential current and charge densities are also related via the continuity equation,

$$\mathbf{F} \mathbf{D} \mathbf{J}_\Delta + jk_0 c_0 \mathbf{I} \rho_\Delta = \mathbf{0}, \quad (7)$$

where \mathbf{I} is the identity matrix. Definitions of the sparse matrices \mathbf{D} , \mathbf{B} and \mathbf{F} may be found in [27].

C. Final System Matrix

The goal now is to utilize equations (2) and (4)–(7) to derive a well-conditioned final system matrix. First, the tangential electric field \mathbf{E} is expressed in terms of the tangential magnetic field \mathbf{H} with a rearrangement of (2),

$$\mathbf{E} = \underbrace{\frac{-1}{j\omega\varepsilon} (\mathbf{L})^{-1} \left(\mathbf{K} - \frac{1}{2} \mathbf{I}_\times \right)}_{\triangleq \mathbf{Z}} \mathbf{H}. \quad (8)$$

Next, the equivalent tangential magnetic field \mathbf{H}_{eq} is expressed in terms of \mathbf{E} with a rearrangement of (5),

$$\mathbf{H}_{\text{eq}} = \underbrace{\frac{1}{j\omega\mu_l} (\mathbf{L}_{\text{eq}})^{-1} \left(\mathbf{K}_{\text{eq}} - \frac{1}{2} \mathbf{I}_\times \right)}_{\triangleq \mathbf{Y}_{\text{eq}}} \mathbf{E}. \quad (9)$$

Matrices \mathbf{Z} and \mathbf{Y}_{eq} may be interpreted, respectively, as the surface impedance of the original object [9] and the surface admittance of the object replaced with the surrounding medium [19].

Using (8) in (9), we may express \mathbf{H}_{eq} in terms of \mathbf{H} as

$$\mathbf{H}_{\text{eq}} = \mathbf{Y}_{\text{eq}} \mathbf{Z} \mathbf{H}. \quad (10)$$

Equations (4), (8) and (10) now allow us to write (6) and (7) in terms of only \mathbf{H} and ρ_Δ , to obtain the final system

$$\begin{bmatrix} jk_0 \mathbf{L}_m^{(A)} + \mathbf{C} & \mathbf{D}^T \mathbf{L}_m^{(\phi)} \mathbf{B} \\ \mathbf{F} \mathbf{D} (\mathbf{I} - \mathbf{Y}_{\text{eq}} \mathbf{Z}) & jk_0 \mathbf{I} \end{bmatrix} \begin{bmatrix} \mathbf{H} \\ c_0 \rho_\Delta \end{bmatrix} = \begin{bmatrix} \mathbf{E}_{\text{inc}} / \eta_0 \\ \mathbf{0} \end{bmatrix}, \quad (11)$$

where

$$\mathbf{C} = \left(-jk_0 \mathbf{L}_m^{(A)} \mathbf{Y}_{\text{eq}} + \eta_0^{-1} \mathbf{I}_\times \right) \mathbf{Z}. \quad (12)$$

Equation (11) is the proposed SLIM formulation. The top left block of (11) has a similar form to the corresponding matrix block in the augmented GIBC formulation [10], but with a different definition of the matrix \mathbf{C} , which may be interpreted as a correction to the well-conditioned vector potential operator for perfect electric conductors, $jk_0 \mathbf{L}_m^{(A)}$. It has been shown that the GIBC formulation leads to a well-conditioned system matrix without the need for dual basis functions [16], and the similarity to this form is responsible for the good conditioning of the SLIM method compared to existing single-source BEM formulations [19], [23]. In particular, $\mathbf{L}_m^{(A)}$, which is well conditioned [28], has a dominant contribution to the overall conditioning of the system in (11), compared to the “correction” matrix \mathbf{C} , which accounts for the finite conductivity of the object. The dominance of $\mathbf{L}_m^{(A)}$ implies that even though some terms in \mathbf{C} are not well tested, for example \mathbf{I}_\times , their impact is diminished, and the use of dual basis functions can be avoided. The same is true for the GIBC, as confirmed in Section III.

Additionally, the SLIM formulation avoids the double-layer potential operator for the exterior problem, required in the GIBC. For objects embedded in stratified media, the single-layer potential involves the dyadic multilayer Green’s function (MGF), while the double-layer potential involves its curl [13]. Avoiding the double-layer operator precludes the need to compute the curl of the MGF, which leads to a significant reduction in CPU time. This feature also reduces code complexity, since the extraction of singular and quasistatic terms for the curl of the MGF is more challenging than for the MGF alone [29].

Although the SLIM formulation requires an additional matrix operator \mathbf{Y}_{eq} in the interior problem, this operator involves the homogeneous Green’s function, which is cheaper to compute than the MGF. Furthermore, for large objects, the inversions in (8) and (9) can be avoided by applying \mathbf{Z} and \mathbf{Y}_{eq} iteratively with the multiple-grid adaptive integral method (AIM) [30] presented in [16]. To efficiently solve (11) with an iterative solver, the constraint preconditioner in [27] is adopted. The matrix-vector product in (11) is accelerated with a multilayer version of the AIM [31].

For structures with multiple objects, matrices \mathbf{Z}_i and $\mathbf{Y}_{i,\text{eq}}$ are independently constructed for each object i . For assembling \mathbf{Z}_i using (8), the properties and Green’s function associated to the material of the i^{th} object are used. For $\mathbf{Y}_{i,\text{eq}}$, the properties and Green’s function associated to the material surrounding the i^{th} object are used. A block diagonal concatenation of all \mathbf{Z}_i and $\mathbf{Y}_{i,\text{eq}}$ provides \mathbf{Z} and \mathbf{Y}_{eq} as

$$\mathbf{Z} = \text{diag} [\mathbf{Z}_1 \quad \mathbf{Z}_2 \dots \mathbf{Z}_{N_{\text{obj}}}], \quad (13)$$

$$\mathbf{Y}_{\text{eq}} = \text{diag} [\mathbf{Y}_{1,\text{eq}} \quad \mathbf{Y}_{2,\text{eq}} \dots \mathbf{Y}_{N_{\text{obj}},\text{eq}}], \quad (14)$$

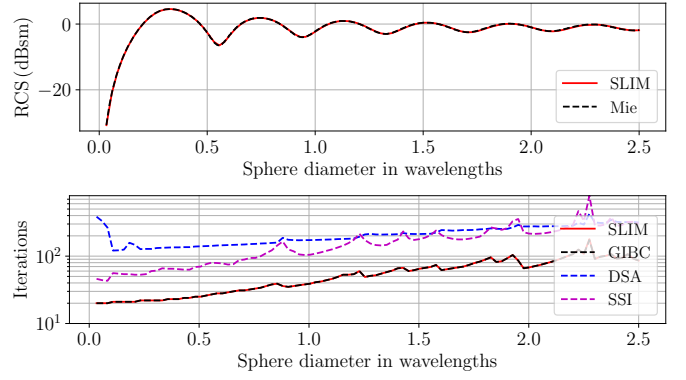


Fig. 1: Top panel: monostatic RCS compared to analytical results. Bottom panel: number of iterations for the proposed, GIBC, DSA and SSI methods, for the sphere in Section III-A.

where N_{obj} is the number of objects. Matrices \mathbf{Z} and \mathbf{Y}_{eq} can then be used directly in (11) and (12).

III. RESULTS

The proposed method is compared to the GIBC [9], DSA [19] and SSI [23] formulations through numerical examples. In each formulation, the AEFIE is used in the exterior problem [10], [31], and the interior problem is accelerated by the method in [16]. All simulations were run single-threaded on a 3 GHz Intel Xeon CPU. We used PETSc [32] for sparse matrix manipulation. The GMRES iterative solver [33] with a relative residual norm of 10^{-4} was used for solving (11).

A. Scattering from a Copper Sphere

To validate the accuracy of the proposed method, a copper sphere ($\sigma = 5.8 \times 10^7$ S/m) with diameter 1 m is considered, meshed with 1,956 triangles and 2,934 edges. The structure is excited with a plane wave at frequencies ranging from 10 MHz to 750 MHz, in free space. The monostatic radar cross section (RCS) is computed and compared with the analytical solution obtained via Mie series [7]. The top panel of Fig. 1 indicates an excellent agreement over the entire range of frequencies considered. The bottom panel of Fig. 1 shows the number of iterations required at each frequency, for the SLIM, GIBC, DSA and SSI approaches. It is clear that the SLIM and GIBC methods lead to significantly better matrix conditioning than the DSA and SSI formulations.

B. Inductor Array

Next, we consider a 3×4 array of copper inductor coils, excited via a Thévenin-equivalent port formulation [24], with ports defined as shown in Fig. 2. Each inductor is a $4 \times$ scaled version of the geometry considered in [20]. The inductors are embedded in the centre of a $50 \mu\text{m}$ dielectric layer with relative permittivity 2.1. Beneath the dielectric layer is a PEC-backed $50 \mu\text{m}$ layer of silicon with relative permittivity 11.9 and conductivity 10 S/m. The structure is meshed with 22,862 triangles and 34,293 edges. Scattering parameters computed over a broad frequency range are shown in Fig. 3, and are

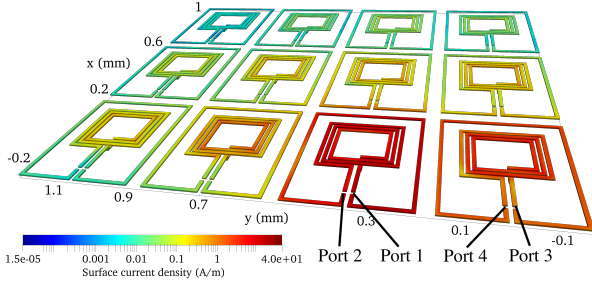


Fig. 2: Geometry of the inductor array in Section III-B, with the electric surface current density at 30 GHz.

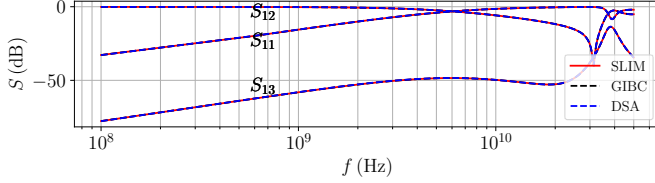


Fig. 3: Comparison of S parameters for the inductor array in Section III-B.

in excellent agreement with both the GIBC and DSA formulations. The maximum error in S_{11} , S_{12} and S_{13} is -75 dB, -72 dB and -74 dB, respectively, compared to the GIBC. The number of GMRES iterations required for convergence are reported in the top panel of Fig. 4, which again highlights that the proposed formulation is as well conditioned as the GIBC, while the SSI formulation failed to converge within 800 iterations. Furthermore, as shown in the bottom panel of Fig. 4, the SLIM formulation is faster than the GIBC since it does not require computing the double-layer potential operator in the outer problem. In total, the SLIM formulation is over $2\times$ faster than both the GIBC and the DSA formulations.

C. On-Chip Interconnect Network

Finally, we consider an on-chip interconnect network consisting of 80 copper signal lines and a ground plane, embedded in a $27.5\ \mu\text{m}$ thick dielectric layer with a relative permittivity of 4 (courtesy of Dr. Rubaiyat Islam, Advanced Micro Devices). Beneath the dielectric layer is a PEC-backed $500\ \mu\text{m}$ layer of silicon with relative permittivity 11.9 and conductivity of $10\ \text{S/m}$. The structure is meshed with 156,820 triangles and 235,230 edges. The geometry, port definitions and electric surface current density at 1 GHz are shown in Fig. 5. The S parameters reported in the top panel of Fig. 6 confirm the accuracy of the SLIM formulation compared to the GIBC method. The maximum error in S_{11} and S_{12} is -37 dB and -33 dB, respectively. The DSA and SSI formulations failed to converge within 800 iterations, and therefore are not included in the results. The bottom panel of Fig. 6 confirms that the proposed method is faster than the GIBC by a factor of over $2\times$, averaged over all frequency points.

IV. CONCLUSION

A novel single-source boundary element formulation is proposed for modeling lossy conductors in layered media.

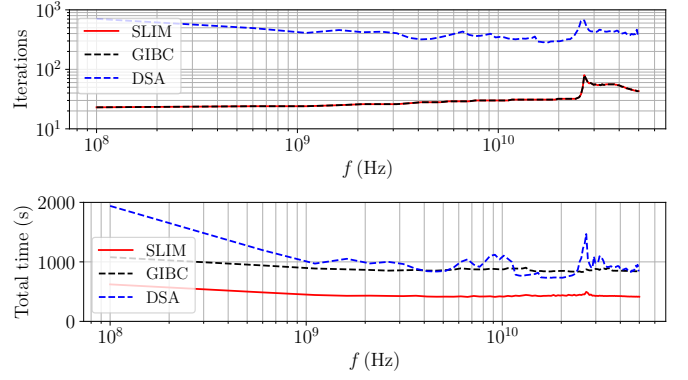


Fig. 4: Performance comparison for the inductor array in Section III-B. Top panel: iterative solver convergence. Bottom panel: total simulation time.

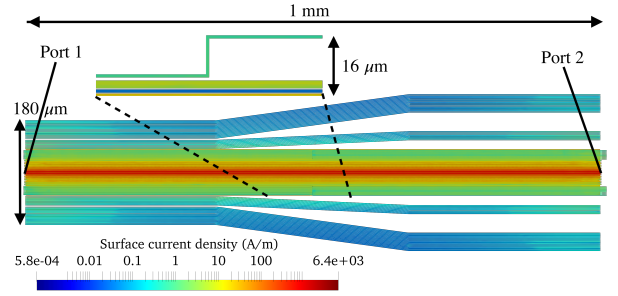


Fig. 5: Geometry of the interconnect network in Section III-C, with the electric surface current density at 1 GHz.

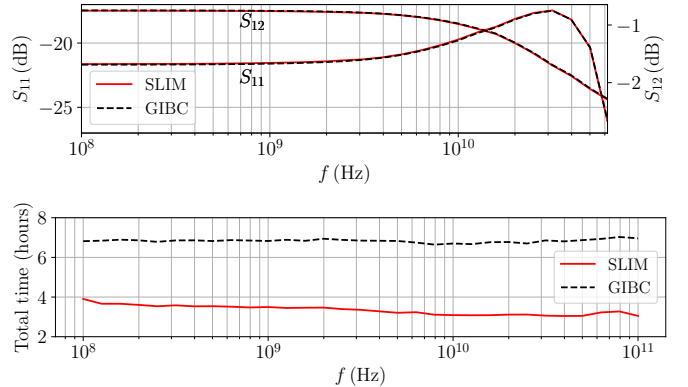


Fig. 6: Comparison of the SLIM and GIBC methods for the interconnect network in Section III-C. Top panel: S parameters. Bottom panel: total simulation time.

Unlike existing techniques, the proposed formulation is well-conditioned without the need for dual basis functions, and avoids the double-layer potential in the exterior problem, making it more efficient when the background medium is modeled with the multilayer Green's function. Numerical examples demonstrate that the proposed technique is more efficient than existing single- and dual-source techniques by a factor of at least $2\times$.

REFERENCES

- [1] C. R. Paul, *Analysis of Multiconductor Transmission Lines*. Hoboken, NJ, USA: Wiley, 2nd ed., 2007.
- [2] D. Güney, T. Koschny, and C. M. Soukoulis, "Reducing ohmic losses in metamaterials by geometric tailoring," *Phys. Rev. B*, vol. 80, p. 125129, Sep. 2009.
- [3] J.-M. Jin, *The Finite Element Method in Electromagnetics*. Hoboken, NJ, USA: Wiley, 3rd ed., 2014.
- [4] S. Omar and D. Jiao, "A new volume integral formulation for broadband 3-D circuit extraction in inhomogeneous materials with and without external electromagnetic fields," *IEEE Trans. Microw. Theory Tech.*, vol. 61, pp. 4302–4312, Dec. 2013.
- [5] A. E. Ruehli, G. Antonini, and L. Jiang, *Circuit Oriented Electromagnetic Modeling Using the PEEC Techniques*. IEEE Press, 2017.
- [6] T. Moselhy, X. Hu, and L. Daniel, "pFFT in FastMaxwell: A fast impedance extraction solver for 3D conductor structures over substrate," in *Proc. Conf. Des., Automat. Test*, 2007.
- [7] W. C. Gibson, *The Method of Moments in Electromagnetics*. Boca Raton, FL, USA: CRC press, 2014.
- [8] S. V. Yuferev and N. Ida, *Surface Impedance Boundary Conditions: A Comprehensive Approach*. Boca Raton, FL, USA: CRC Press, 2009.
- [9] Z. G. Qian, W. C. Chew, and R. Suaya, "Generalized impedance boundary condition for conductor modeling in surface integral equation," *IEEE Trans. Microw. Theory Tech.*, vol. 55, pp. 2354–2364, Nov. 2007.
- [10] Z.-G. Qian, M. S. Tong, and W. C. Chew, "Conductive medium modeling with an augmented GIBC formulation," *Prog. Electromagn. Res.*, vol. 99, pp. 261–272, 2009.
- [11] W. Chai and D. Jiao, "Direct matrix solution of linear complexity for surface integral-equation-based impedance extraction of complicated 3-D structures," *Proc. IEEE*, vol. 101, pp. 372–388, Jun. 2013.
- [12] D. Colton and R. Kress, *Integral Equation Methods in Scattering Theory*. Hoboken, NJ, USA: Wiley, 1983.
- [13] K. A. Michalski and J. R. Mosig, "Multilayered media Green's functions in integral equation formulations," *IEEE Trans. Antennas Propag.*, vol. 45, pp. 508–519, Mar. 1997.
- [14] T. Xia, H. Gan, M. Wei, W. C. Chew, H. Braunisch, Z. Qian, K. Aygün, and A. Aydin, "An integral equation modeling of lossy conductors with the enhanced augmented electric field integral equation," *IEEE Trans. Antennas Propag.*, vol. 65, pp. 4181–4190, Aug. 2017.
- [15] A. Buffa and S. H. Christiansen, "A dual finite element complex on the barycentric refinement," *Math. Computation*, vol. 76, pp. 1743–1769, 2007.
- [16] S. Sharma and P. Triverio, "A fully-accelerated surface integral equation method for the electromagnetic modeling of arbitrary objects," *IEEE Trans. Antennas Propag.*, 2020 (submitted, arXiv: 2003.11679).
- [17] D. De Zutter and L. Knockaert, "Skin effect modeling based on a differential surface admittance operator," *IEEE Trans. Microw. Theory Tech.*, vol. 53, pp. 2526 – 2538, Aug. 2005.
- [18] M. Huynen, K. Y. Kapusuz, X. Sun, G. Van der Plas, E. Beyne, D. De Zutter, and D. Vande Ginste, "Entire domain basis function expansion of the differential surface admittance for efficient broadband characterization of lossy interconnects," *IEEE Trans. Microw. Theory Tech.*, vol. 68, pp. 1217–1233, Jan. 2020.
- [19] U. R. Patel, S. V. Hum, and P. Triverio, "A novel single-source surface integral method to compute scattering from dielectric objects," *IEEE Antennas Wireless Propag. Lett.*, vol. 16, pp. 1715–1718, Feb. 2017.
- [20] U. R. Patel, S. Sharma, S. Yang, S. V. Hum, and P. Triverio, "Full-wave electromagnetic characterization of 3D interconnects using a surface integral formulation," in *IEEE Conf. Electr. Perform. Electron. Packag. and Syst.*, (San Jose, CA), Oct. 2017.
- [21] S. Sharma and P. Triverio, "A well-conditioned differential surface admittance formulation for modeling penetrable media," in *IEEE Int. Symp. Antennas Propag. USNC-URSI Radio Sci. Meeting*, pp. 1673–1674, Jul. 2019.
- [22] M. Gossye, M. Huynen, D. Vande Ginste, D. De Zutter, and H. Rogier, "A Calderón preconditioner for high dielectric contrast media," *IEEE Trans. Antennas Propag.*, vol. 66, pp. 808–818, Feb. 2018.
- [23] S. Sharma and P. Triverio, "A single-source surface impedance formulation for modeling arbitrary penetrable media," in *IEEE Int. Symp. Antennas Propag. USNC-URSI Radio Sci. Meeting*, Jul. 2020.
- [24] Y. Wang, D. Gope, V. Jandhyala, and C.-J. R. Shi, "Generalized Kirchhoff's current and voltage law formulation for coupled circuit-electromagnetic simulation with surface integral equations," *IEEE Trans. Microw. Theory Tech.*, vol. 52, pp. 1673–1682, Jul. 2004.
- [25] S. Rao, D. Wilton, and A. Glisson, "Electromagnetic scattering by surfaces of arbitrary shape," *IEEE Trans. Antennas Propag.*, vol. 30, pp. 409–418, May 1982.
- [26] R. F. Harrington, *Time-Harmonic Electromagnetic Fields*. Hoboken, NJ, USA: Wiley, 1961.
- [27] Z.-G. Qian and W. C. Chew, "Fast full-wave surface integral equation solver for multiscale structure modeling," *IEEE Trans. Antennas Propag.*, vol. 57, pp. 3594–3601, Nov. 2009.
- [28] G. C. Hsiao and R. E. Kleinman, "Mathematical foundations for error estimation in numerical solutions of integral equations in electromagnetics," *IEEE Trans. Antennas Propag.*, vol. 45, pp. 316–328, Mar. 1997.
- [29] E. Simsek, Q. H. Liu, and B. Wei, "Singularity subtraction for evaluation of green's functions for multilayer media," *IEEE Trans. Microw. Theory Tech.*, vol. 54, pp. 216–225, Jan. 2006.
- [30] E. Bleszynski, M. Bleszynski, and T. Jaroszewicz, "AIM: Adaptive integral method for solving large-scale electromagnetic scattering and radiation problems," *Radio Sci.*, vol. 31, pp. 1225–1251, Sep. 1996.
- [31] S. Sharma, U. R. Patel, S. V. Hum, and P. Triverio, "A complete surface integral method for broadband modeling of 3D interconnects in stratified media," *arXiv e-prints*, p. arXiv: 1810.04030, Oct. 2018.
- [32] S. Balay, S. Abhyankar, M. F. Adams, J. Brown, P. Brune, K. Buschelman, L. Dalcin, V. Eijkhout, W. D. Gropp, D. Kaushik, M. G. Knepley, D. A. May, L. C. McInnes, R. T. Mills, T. Munson, K. Rupp, P. Sanan, B. F. Smith, S. Zampini, H. Zhang, *PETSc Web Page*. (2019). Accessed: Nov. 01, 2019. Available: <http://www.mcs.anl.gov/petsc>.
- [33] Y. Saad and M. Schultz, "GMRES: A generalized minimal residual algorithm for solving nonsymmetric linear systems," *SIAM J. Scientific Statistical Comput.*, vol. 7, no. 3, pp. 856–869, 1986.